Talanta 119 (2014) 24–33

Contents lists available at ScienceDirect

Talanta

journal homepage: www.elsevier.com/locate/talanta

Development of a new biosensor based on functionalized SBA-15 modified screen-printed graphite electrode as a nano-reactor for Gquadruplex recognition

Zahra Bagheryan [a], Jahan-Bakhsh Raoof [a,*], Reza Ojani [a], Parizad Rezaei [b]

[a] Eletroanalytical Chemistry Research Laboratory, Department of Analytical Chemistry, Faculty of Chemistry, University of Mazandaran, Babolsar, Iran
[b] Department of Organic Chemistry, Faculty of Chemistry, University of Mazandaran, Babolsar, Iran

ARTICLE INFO

Article history:
Received 17 June 2013
Received in revised form
25 September 2013
Accepted 27 September 2013
Available online 31 October 2013

Keywords:
Gquadruplex DNA
Electrochemical biosensor
Ascorbic acid
Mesoporous structure
Genomic studies

ABSTRACT

Gquadruplex is an active target for therapeutic purposes because of the evidence which suggest that G-rich region of the human genome may form Gquadruplex structure. The electrochemical biosensor was prepared by modifying screen-printed graphite electrode (SPE) with synthesized SBA-*N*-propylpi-pyrazine-*N*-(2-mercaptopropane-1-one) (SBA@NPPNSH) mesoporous structure to investigate the Gquadruplex DNA structure (G_4DNA). Ascorbic acid (AA) is known as an antioxidant agent that induces reductive properties. It is also important for some therapeutic purposes. In this study, AA was used as the model ligand and its ability to interact with Gquadruplex structure was examined. The pore of SBA@NPPNSH structure can act as a nano-reactor and the interaction of G_4DNA/AA is accomplished inside these channels. The structure of SBA@NPPNSH was characterized by transmission electron microscope (TEM), X-ray powder diffraction (XRD), thermo gravimetric analysis (TGA) methods and atomic force microscopy (AFM). The interaction of AA with G_4DNA was studied in Tris–HCl buffer and also in the presence of $[Fe(CN)_6]^{3-}$ as a redox label using the CV method. CV current decreases with the increasing concentrations of AA due to the interaction of G_4DNA/AA. Circular dichroism (CD) spectroscopy was used to examine the ability of AA to form Gquadruplexes from short and long complementary G_4DNA strands. Studying the selectivity using different dsDNA sequences revealed that AA could stabilize G_4DNA. Thus, the proposed biosensor can distinguish G_4DNA structure from other dsDNA structures.
© 2013 Elsevier B.V. All rights reserved.

1. Introduction

Telomeres are the special DNA/protein structures at the end of chromosomes that are essential to stabilize genome [1] and appear to play an important role in cellular aging and cancer [2]. Human telomeric DNA typically consists of a duplex region composed of TTAGGG repeated units, ending in a 100–200 nucleotide guanine-rich single stranded overhang, which termed a four strand Gquadruplex structure involving planer G-quartets (G_4DNA) [3,4]. This structure has been found to inhibit telomerase enzyme activity [5], a cancer specific reverse transcriptase, that is involved in around 80–90% of cancers [6]. Gquadruplex structure makes the telomeric DNA tail inaccessible to telomerase, thus blocks the telomerase reaction and inhibits elongation step [4]. The structure and stability of Gquadruplex depend on monocations such as K^+ and Na^+ [7,8]. This structure has attracted intense interest in recent years because of its relevance to the cancer biology [9], cell division [10], gene expression control [11], genetic recombination [12] and its important role as a target for drug design [13–15]. It is assumed that poor preservation of Gquadruplex structure, which forms at telomeres end, is responsible for a number of human certain cancers and diseases [14,16]. So, it is particularly attractive as a target for anticancer therapeutic development [5] and a good target for drug design. In this regard, choosing a ligand with a good affinity with Gquadruplex to stabilize this structure or induce the folding of this structure of single stranded DNA is a good strategy for cancer therapy, as it can inhibit the activity of telomerase and could be a potential anticancer agent.

Ascorbic acid (AA) is a naturally occurring organic compound with antioxidant properties. Human cannot synthesize AA and require it as a part of his/her nutrition, but many animals are able to produce it. Other vertebrates lacking the ability to produce AA include other primates, guinea pigs, teleost fishes, bats, and birds, all of which require it as a dietary micronutrient (that is, a vitamin) [17].

In the present study, a direct and sensitive electrochemical method was proposed to identify Gquadruplex structure. To this end, graphite screen-printed electrode (SPE) was employed as an inexpensive, rapid, simple and a mass production capable electrode

* Corresponding author. Tel.: +98 112 5342392; fax: +98 112 5342350.
E-mail address: j.raoof@umz.ac.ir (J.-B. Raoof).

0039-9140/$ - see front matter © 2013 Elsevier B.V. All rights reserved.
http://dx.doi.org/10.1016/j.talanta.2013.09.052

[18,19]. Then, it was modified with SBA-*N*-propylpipyrazine-*N*-(2-mercaptopropane-1-one) (SBA@NPPNSH) synthesized mesoporous structure and used in all experiments. AA was selected as a Gquadruplex-binding model ligand and its affinity to G_4DNA was examined using the electrochemical signal change. The properties of synthesized SBA@NPPNSH were identified by AFM, TEM, XRD, and TGA methods. The Gquadruplex formation and interaction mechanism between G_4DNA/AA were also investigated by circular dichroism (CD) spectroscopy method. The potential competition interaction of AA and different size complementary strands of G_4DNA were also investigated, because the formation of Gquadruplex structure competes with double helix structure according to the literature [20].

2. Experimental

2.1. Reagents

All starting materials and reagents for synthesis of SBA@NPPNSH were supplied commercially from Aldrich or Merck Chemical Company. DNA oligonucleotides were purchased from MWG-BIOTECH, Germany, with following base sequences:

Single-stranded human telomeric DNA (ssDNA):

(5′ GGG TTA GGG TTA GGG TTA GGG 3′)

Double stranded probe:

dsDNA (I):

5′-GGG TTA GGG TTA GGG TTA GGG-3′

3′-CCC AAT CCC AAT CCC AAT CCC-5′

dsDNA (II):

5′-GGG TTA GGG TTA GGG TTA GGG-3′

3′-CCC AAT CCC AAT CCC AAT-5′

dsDNA (III):

5′-GGG TTA GGG TTA GGG TTA GGG-3′

3′-CCC AAT CCC AAT CCC-5′

dsDNA (IV):

5′-GGG TTA GGG TTA GGG TTA GGG-3′

3′-CCC AAT CCC AAT-5′

dsDNA (V):

5′-GGG TTA GGG TTA GGG TTA GGG-3′

3′-CCC AAT-5′

The stock solution of DNA (1.0 μmol L^{-1}) was prepared by 50 mmol L^{-1} Tris–HCl buffer (50 mmol L^{-1} Tris–HCl, 1.0 mmol L^{-1} EDTA, pH 8.00) and kept frozen. To make the Gquadruplex structure of human telomeric DNA (G_4DNA), a solution of KCl (100 mmol L^{-1}) was added to ssDNA (1.0 μmol L^{-1}) and it was carefully put in 4 °C for 20 min. Double-stranded DNA (dsDNA)

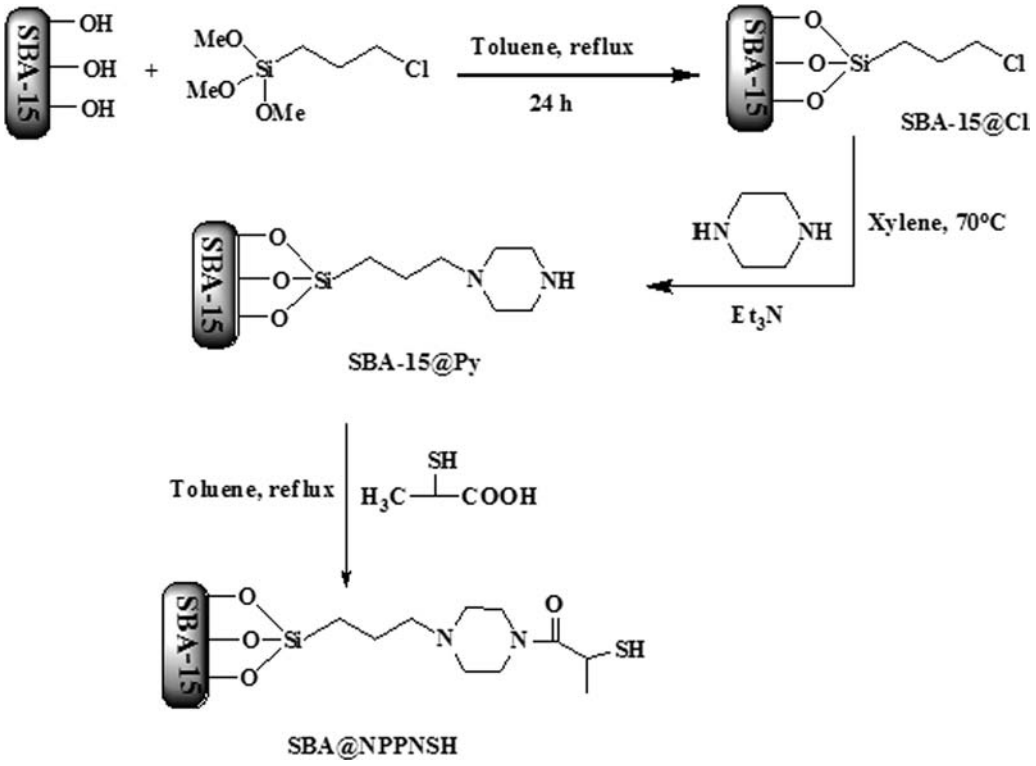

Scheme 1. Synthesis steps of SBA-*N*-propylpipyrazine-*N*-(2-mercaptopropane-1-one). .

formation was carried out by heating a solution containing ssDNA and its complementary sequences at 95 °C for 10 min, in the presence of 50 mmol L^{-1} Tris–HCl and 100 mmol L^{-1} KCl at pH 7.40, followed by slow cooling at room temperature [21]. Double deionized water was used in all experiments. Solution pH was adjusted to 7.40, using hydrogen chloride or sodium hydroxide to preserve physiological conditions.

2.2. Instrumentation

Electrochemical studies were performed using Autolab PGstut 30 electrochemical analysis system, controlled by GPES 4.9 and FRA software (Eco Chemie Netherlands). Screen-printed electrodes (purchased from Florence, Italy) (SPEs) were made of a carbon working electrode, a carbon counter electrode and a silver pseudo reference electrode. Materials and procedures to screen-print the transducers were described elsewhere [22]. CD measurements were made on a Model 215 CD recorder (Aviv, USA) from 320 to 200 nm. Standard quartz cells of 1.0 cm path-length were used for all CD measurements. The circular dichroism nerve network (CDNN) software was used for data analysis. All the experiments were carried out at room temperature. The structure of SBA@NPPNSH was compared with an Easyscan2 Flex Atomic Force Microscopy (AFM, Switzerland), before and after G_4DNA immobilization. Thermo gravimetric analysis (TGA) was recorded on a Stanton Redcraft STA-780 (London, UK). Transmission electron microscopic (TEM) images were observed under the TEM-PHILIPS-CM10HT100KV instrument. X-ray powder diffraction (XRD) patterns of the PIs were recorded by an X-ray diffractometer (XRD, GBC MMA Instrument) with Be-filtered Cu Kα radiation and IR spectra were determined on a Bruker instrument.

2.3. Procedure

2.3.1. Preparation of SBA-N-propylpipyrazine-N-(2-mercaptopropane-1-one):

The mesoporous structure was prepared according to typical heterogeneous process, as outlined in reaction Scheme 1. SBA-15 was prepared according to the procedure known in the literature [23]. In this way, 2.0 g of SBA-15 was first refluxed with 2.0 mL of 3-chloropropyltrimethoxysilane in dry toluene (100 mL) for 24 h. Then, a suspension of SBA-15@Cl (1.0 g) in 100 ml of xylene was allowed to react with piperazine (Py) (0.5 g) in the presence of triethylamine (1.0 mL) as proton abstractor. This process was carried out under continuous stirring and a nitrogen atmosphere for 48 h at 70 °C. The product was filtered and washed with xylene and hot ethanol for 12 h in a continuous extraction apparatus (Soxhlet) and then dried under vacuum [24]. Next, the magnetically stirred mixture

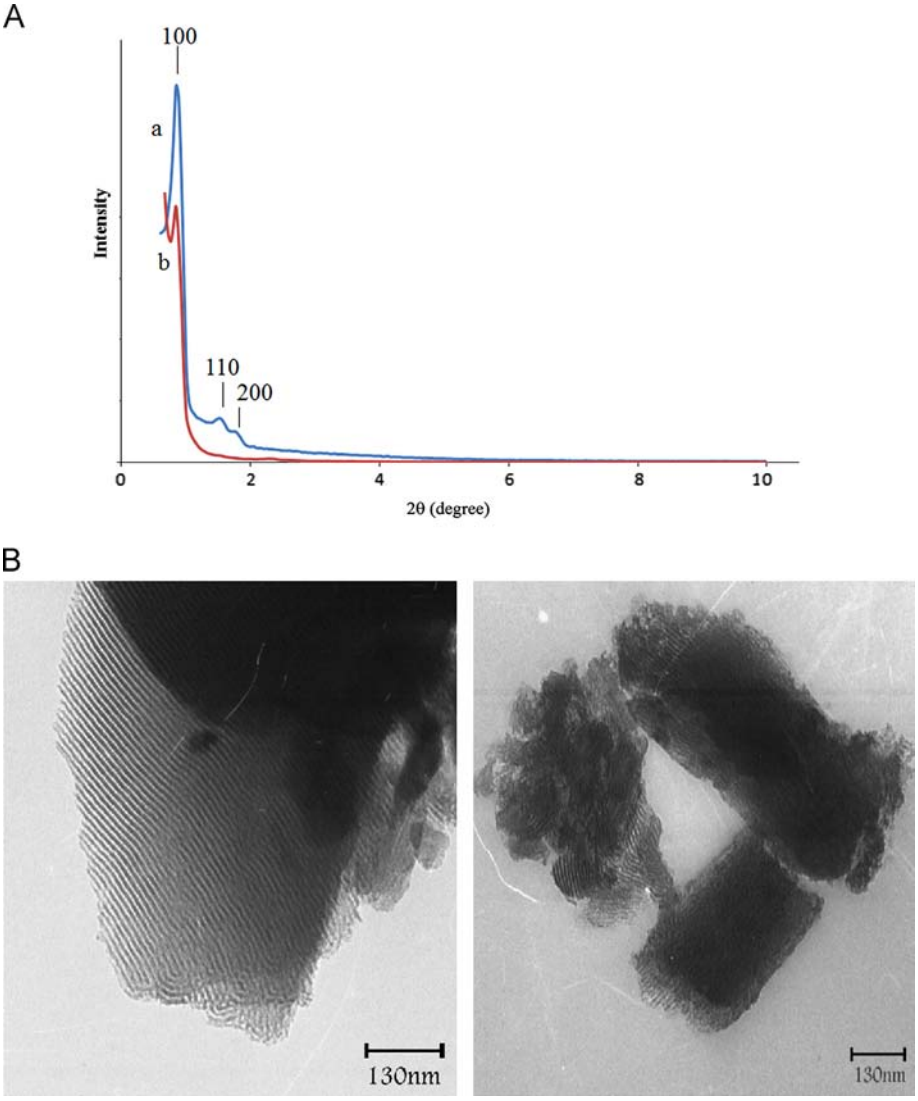

Fig. 1. (A) XRD patterns for (a) SBA-15 and (b) SBA@NPPNSH. (B) TEM image of compound SBA@NPPNSH.

of SBA-15@Py (1.0 g) was refluxed with 2-mercaptopropanoic acid (1.0 mL) in toluene for 24 h. The mixture was filtered by sintered glass funnel and washed with hot toluene for 12 h in a continuous extraction apparatus (Soxhlet) and dried in oven at 110 °C overnight to afford SBA-*N*-propylpipyrazine-*N*-(2-mercaptopropane-1-one) (SBA@NPPNSH). The synthesized SBA@NPPNSH was characterized by TGA, TEM, IR spectra, XRD patterns, N_2 adsorption–desorption and elemental analysis methods.

2.3.2. Preparation of the modified graphite screen-printed electrode

A droplet of 10 μL SBA@NPPNSH was placed on the working electrode surface, followed by air-drying for 1.0 h. Then, it was soaked in ultrapure water to remove unabsorbed SBA@NPPNSH.

2.3.3. Immobilization of G_4DNA on the SBA@NPPNSH/SPE

In order to immobilize G_4DNA, 10 μL drops of 1.0 μmol L^{-1} G_4DNA solutions was deposited on the freshly retreated SBA@NPPNSH/SPE surface, followed by applying +0.50 V potential vs. Ag/AgCl/KCl (3 mol L^{-1}) for 5 min. The electrode was then rinsed with sterilized and deionized water.

Table 1
Textural parameters of prepared. SBA@NPPNSH.

Sample	SBET (m^2 g^{-1})	*V* (cm^3 g^{-1})	DBJH (nm)
SBA-15	709	0.8728	6.5
SBA@NPPNSH	114	0.1896	4.9

SBET is the BET surface area; *V* is the total pore volume; DBJH is the average porediameter calculated using BJH method.

2.3.4. Interaction of G_4DNA with ascorbic acid on the surface of working electrode

the interaction of G_4DNA with AA on the working electrode surface was investigated in three steps. First G_4DNA was immobilized at the SBA@NPPNSH/SPE as mentioned in Section 2.3.3. Second the immobilized G_4DNA/SBA@NPPNSH/SPE was immersed in ligand solution. Thired the cyclic voltammetry measurements were recorded in the range −0.5 and +1.2 V vs. Ag/AgCl/KCl (3 mol L^{-1}) at scan rate of 50 mV s^{-1}.

3. Results and discussion

3.1. Analysis of the SBA@NPPNSH

Fig 1A shows the low angle XRD patterns of SBA-15 and the functionalized SBA-15 (SBA@NPPNSH). All the samples have a single intensive reflection at 2θ angle around 0.86° similar to the typical SBA-15 materials, which is generally attributed to the long-range periodic [25]. Two additional peaks corresponding to the higher ordering (110) and (200) reflections are also observed for the SBA-15 material, which is associated with a two-dimensional hexagonal (p6 mm) structure.

Fig. 1B illustrates TEM images of SBA@NPPNSH. The TEM image reveals the parallel channels, which resemble the porous configuration of SBA-15. This indicates that the pores of SBA@NPPNSH were not collapsed during the three steps of reactions, which is in good agreement with the XRD results.

The textural properties of the samples were evaluated from the nitrogen adsorption–desorption isotherms (Supplementary material, Fig. S1A and S1B). The respective specific surface areas (BET

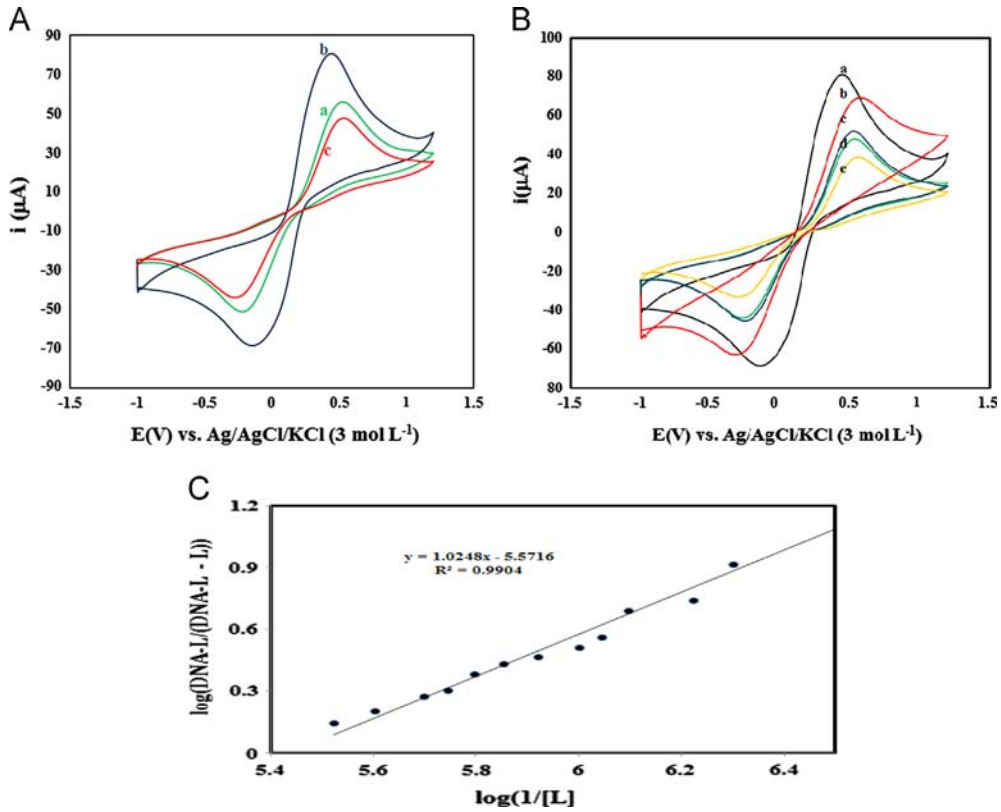

Fig. 2. (A) Cyclic voltammgrames of (a) SPE, (b) SBA@NPPNSH/SPE and (c) G_4DNA/SBA@NPPNSH/SPE. (B) CVs of G_4DNA/SBA@NPPNSH/SPE electrodes in the absence (a) and presence of different concentrations of AA: 1.0×10^{-7} mol L^{-1} (b), 1.0×10^{-6} mol L^{-1} (c), 1.0×10^{-5} mol L^{-1} (d) and 1.0×10^{-4} mol L^{-1} (e) in 0.5 mmol L^{-1} $[Fe(CN)_6]^{3-}$ and 100 mmol L^{-1} KCl at a scan rate of 50 mV s^{-1}. (C) A plot of Log ($I_{DNA-L}/I_{DNA}-I_{DNA-L}$) vs. Log (1/[*L*]) for determination binding constant.

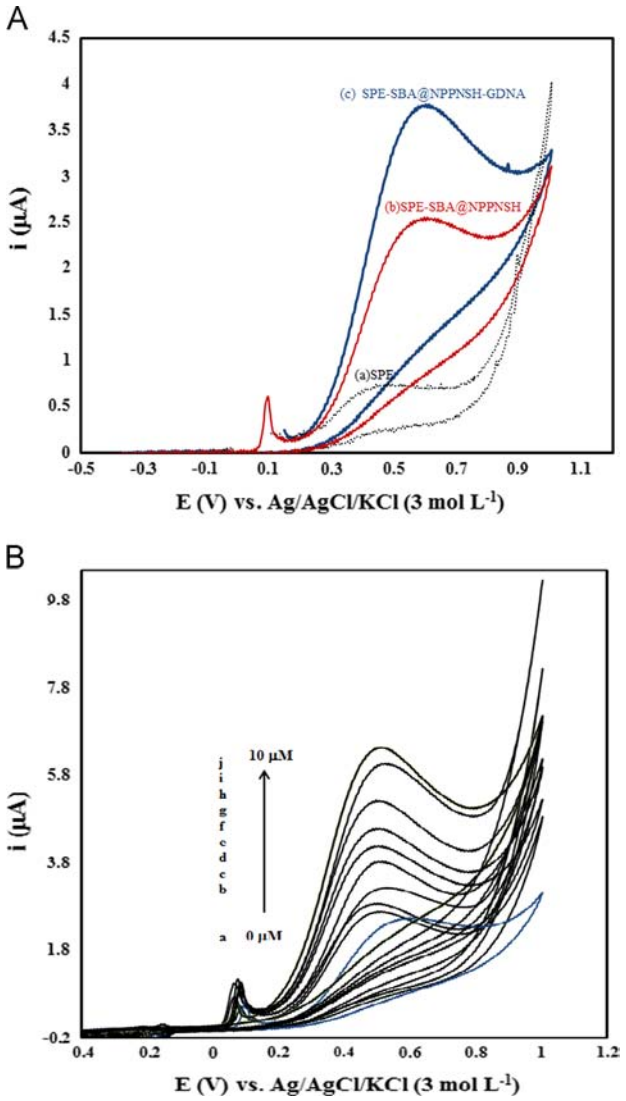

Fig. 3. (A) CV signals of 1×10^{-4} mol L^{-1} AA in a 50 mmol L^{-1} Tris–HCl solution in the presence of SPE (a), SBA@NPPNSH/SPE (b) and G_4DNA/SBA@NPPNSH/SPE (c) at a scan rate of 50 mV s^{-1}. (B) CV signals of 1×10^{-4} mol L^{-1} AA in a 50 mmol L^{-1} Tris–HCl solution before (a) and after immobilization of different concentration of G_4DNA 0.3 μmol L^{-1} (b), 0.6 μmol L^{-1} (c), 0.9 μmol L^{-1} (d), 2 μmol L^{-1} (e), 4 μmol L^{-1} (f), 6 μmol L^{-1} (g), 8 μmol L^{-1} (h), 10 μmol L^{-1} (i) and 12 μmol L^{-1} (j) at SBA@NPPNSH/SPE.

method), pore diameters (BJH method) and total pore volumes are given in Table 1.

The isotherms show a type-IV isotherm with an obvious H1-type hysteresis loop that is representative of the mesoporous cylindrical or rod-like pores. These results clearly indicate that the mesostructure is preserved during the surface modification. It is noteworthy to say that the specific surface area, total pore volume and average pore diameter of samples decrease as the extent of organic lining increases, which indicate that a major surface modification takes place on the surface of SBA-15 nano channels.

The incorporation of organic functional groups in the SBA-15 framework was confirmed by FT-IR spectra (Fig. S2A). In the FT-IR spectra, peaks around 3500–3300, 2933, 2553, 1660–1550 and 1250–1040 cm^{-1} are due to O–H of silanols, C–H stretching vibrations, S–H stretching vibrations, overlapped free OH, C=O groups and Si–O–Si stretching vibrations, respectively.

The chemical compositions of the organo-functional groups, covalently linked to mesoporous silica materials, were determined by elemental analysis. After drying SBA@NPPNSH under vacuum, the quantity of mercapto groups attached to it (1.62 mmol/g) was calculated by elemental analysis (CHNS), from the sulfur percentage (5.18%). The grafted amount of organic species, which was determined by TGA analysis (Fig. S2B), is in good agreement with the results (determination of organic content) obtained by elemental analysis. Typically, a loading at ca. 1.70 mmol/g for surface bound group was obtained.

3.2. Electrochemical study of G_4DNA interaction with AA by using $[Fe(CN)_6]^{3-}$ as a redox marker

The quality of G_4DNA immobilization on the electrode surface was evaluated by CV measurement in 50 mmol L^{-1} Tris–HCl buffer solutions (pH 7.40), containing 0.01 mol L^{-1} $[Fe(CN)_6]^{3-}$ and 100 mmol L^{-1} KCl, at scan rate of 50 mV s^{-1} (Fig. 2A). As is shown in Fig. 2A, the intensity of $[Fe(CN)_6]^{3-}$ signal increases significantly after depositing SBA@NPPNSH on the electrode surface (curve b). Indeed, the porous structure of SBA@NPPNSH and its high electrical conductivity leads to an increase in $[Fe(CN)_6]^{3-}$ redox signal intensity compared to that of bare electrode (curve a). Apparently, the SBA@NPPNSH/SPE has higher effective surface area so it can significantly enhance the electron transfer as a mediator and induces higher bioactivity owing to the intensified surface area. It can be observed from (curve c) that when G_4DNA is immobilized onto the SBA@NPPNSH modified surface, a first layer is formed. Binding G_4DNA decreases the redox peak current of $[Fe(CN)_6]^{3-}$ with increasing its ΔE_p (curve c). The charge repulsion between the negatively charged phosphate backbone of G_4DNA and the $[Fe(CN)_6]^{3-}$ electrochemical label results in reduction of electron transfer on the electrode surface and so, have a decreasing effect on redox signal.

In the next phase of the study, the electrochemical response of G_4DNA/SBA@NPPNSH/SPE was studied in the presence of AA in $[Fe(CN)_6]^{3-}$ solution. Fig. 2B shows the cyclic voltammetric response curves of the G_4DNA/SBA@NPPNSH/SPE in $[Fe(CN)_6]^{3-}$ solution when interacted with different concentrations of AA (Fig. 2B). It is shown that increasing the AA concentration will decrease the CV peak current. The results indicate that the reduced intensity of peak is due to the specific interaction between G_4DNA and AA.

It is assumed that G_4DNA and ligand produce only a single complex, DNA–ligand.

$$G_4DNA + mL \leftrightarrow G_4DNA - L_m$$

The value of the binding constant for the interaction of AA with G_4DNA is determined using Eq. (1) as described by Ibrahim [26]. The modified equation in the litreture [27] was used with little change as follows:

$$\log \frac{I_{DNA-L}}{I_{DNA}-I_{DNA-L}} = -\log K_b + m \log \frac{1}{[L]} \quad (1)$$

where K_b is the apparent binding constant, I_{DNA} is the peak current of immobilized G_4DNA alone, L is ligand (AA), and I_{DNA-L} is the peak current of G_4DNA after interaction with AA. If G_4DNA and ligand form a single complex, the plot of $(I_{DNA}-L/(I_{DNA}-I_{DNA-L}))$ vs. log $(1/[L])$ becomes linear with slope m and intercept K_b. According to Eq. (1), a plot of log $(I_{DNA}-L/(I_{DNA}-I_{DNA-L}))$ against log $(1/[L])$ result in a straight line (Fig. 2C), the intercept of which being equal to the logarithm of binding constant. The K_b value, thus calculated, found to be 3.7×10^5 mol L^{-1}.

3.3. Electrochemical study of G_4DNA on SBA@NPPNSH/SPE by using AA oxidation peak

The interaction mechanism of AA with G_4DNA was investigated by electrochemical methods at a G_4DNA/SBA@NPPNSH/SPE. AA is an electroactive substance which represents an anodic peak in the cyclic

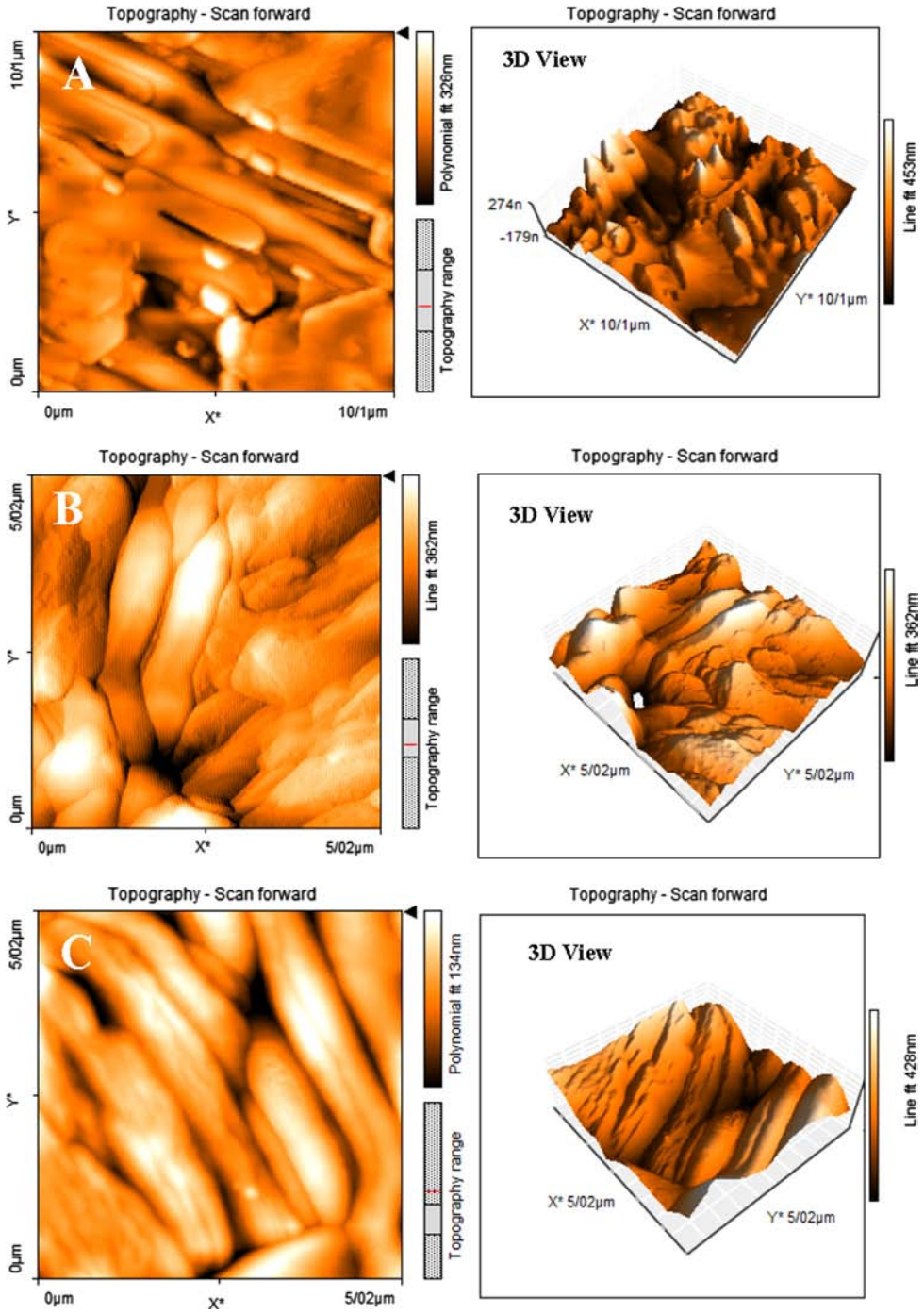

Fig. 4. AFM image of SBA@NPPNSH (A); G_4DNA/SBA@NPPNSH (B) and dsDNA (I)/SBA@NPPNSH (C).

voltammogram. Fig. 3A shows the cyclic voltammogram of 1.0×10^{-4} mol L^{-1} AA at a bare SPE (curve a), modified SPE with SBA@NPPNSH (curve b) and G_4DNA-modified SBA@NPPNSH/SPE (curve c), in 0.01 mol L^{-1} Tris–HCl (pH 7.40) buffer solution. Comparing curves (a) and (b) in Fig. 3A illustrates that the SBA@NPPNSH can catalyze the electrooxidation of AA and significantly enhances its oxidation peak current as a mediator. Thus, SBA@NPPNSH is capable of carrying a higher bioactivity which is related to its intense surface area. As can be seen, the height of oxidation peak current of AA increases after G_4DNA immobilization on the modified SPE. It can be explained in this way: the size of G_4DNA structure is suitable for entering in the parallel channels of SBA@NPPNSH. So it can interact with chemical groups inside the channels to become more stable. Therefore, the channels of SBA@NPPNSH can act as nano reactors and G_4DNA preconcentration can be accomplished inside the SBA@NPPNSH channels. In the presence of AA, the interaction of AA/G_4DNA takes place in this nano-size reactor and signal of AA increases significantly. Fig. 3B shows the cyclic voltammogram of 1.0×10^{-4} mol L^{-1} AA, after immobilization of diferent concentration of G_4DNA at modified SBA@NPPNSH/SPE in 0.01 mol L^{-1} Tris–HCl (pH 7.40) buffer solution. As it is clear, the oxidation peak current of AA increases significantly following increasing G_4DNA concentrations.

Moreover, atomic force microscopy (AFM) was employed as additional evidence for G_4DNA immobilization. Fig. 4 represents AFM images of SBA@NPPNSH and G_4DNA/SBA@NPPNSH. Fig. 4A indicates a mesoporous structure for SBA@NPPNSH with nano-size parallel

channel and Fig. 4B shows the morphology of SBA@NPPNSH in the presence of G_4DNA. As can be seen, the porous structure of SBA@NPPNSH, containing high effective surface area, changed to a compact structure in the presence of G_4DNA, which is in good agreement with the results obtained from CV method (decreasing the $[Fe(CN)_6]^{3-}$ peak current after G_4DNA immobilization). It also indicates the spherical protuberance of G_4DNA structure, which is quite different from dumbbell-shaped structure of dsDNA as shown in Fig. 4C. Obviously, the height of the G_4DNA structure is more than that of dsDNA structure, which suggests that the Gquadruplexe structure is formed.

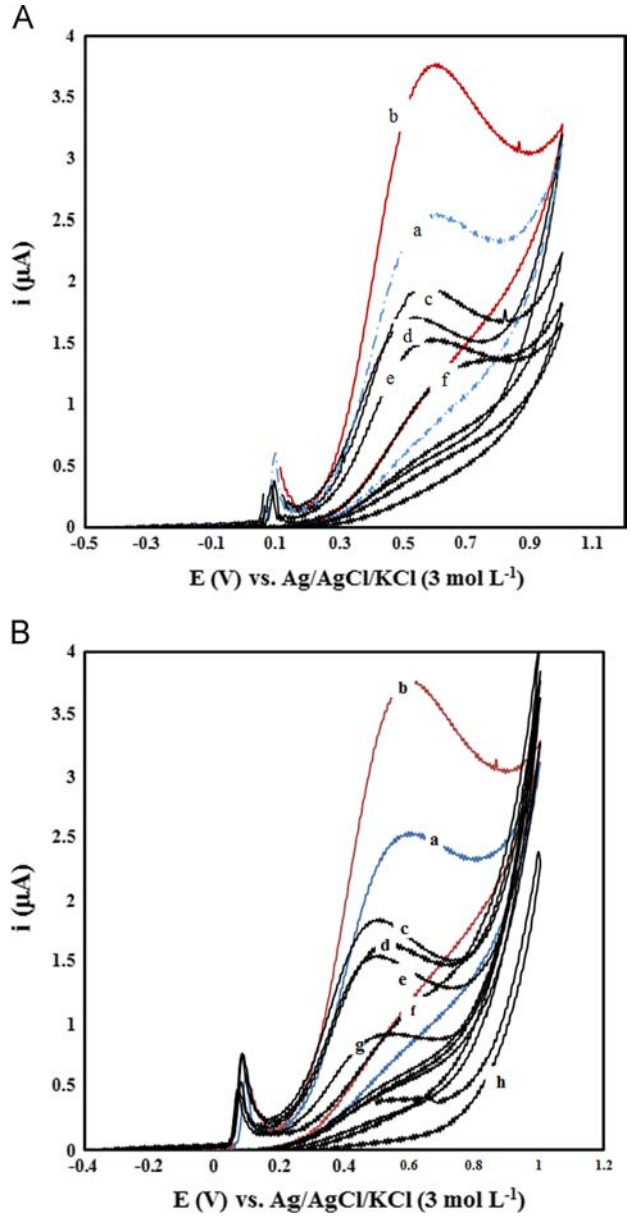

Fig. 5. (A) CV signal of 1×10^{-4} M AA in SBA@NPPNSH/SPE (a), G_4DNA/SBA@NPPNSH/SPE (b), dsDNA (I)/SBA@NPPNSH/SPE (c), dsDNA (II)/SBA@NPPNSH/SPE (curve d), dsDNA (III)/SBA@NPPNSH/SPE (curve e) and dsDNA (IV)/SBA@NPPNSH/SPE (curve f). (B) CV signal of 1×10^{-4} M AA in SBA@NPPNSH/SPE (a), G_4DNA/SBA@NPPNSH/SPE (b), c53c(dsDNA) /SBA@NPPNSH/SPE (c), HPV(dsDNA)/SBA@NPPNSH/SPE (d), g53g(dsDNA)/SBA@NPPNSH/SPE (e), g53g(ssDNA)/SBA@NPPNSH/SPE (f), c53c (ssDNA)/SBA@NPPNSH/SPE (g) and PNA/SBA@NPPNSH/SPE (h) in Tris–HCl buffer solution containing 100 mmol L^{-1} KCl, (pH 7.40) at a scan rate of 50 mV s^{-1} at the surface of electrode.

3.4. Selectivity study

In order to study the selectivity of the proposed biosensor, the modified SPE was treated with some different double stranded (dsDNA) oligonucleotides and G_4DNA. Then, the modified electrodes were immersed in 1.0×10^{-4} mol L^{-1} AA solution and cyclic voltammograms were recorded between −0.5 and +1.2 V vs. Ag/AgCl/KCl (3 mol L^{-1}), at scan rate of 50 mV s^{-1}. Fig. 5 shows CV signals of AA at SBA@NPPNSH/SPE (a), G_4DNA/SBA@NPPNSH/SPE (b), dsDNA (IV)/SBA@NPPNSH/SPE (c), dsDNA (III)/SBA@NPPNSH/SPE (d), dsDNA (II)/SBA@NPPNSH/SPE (e) and dsDNA (I)/SBA@NPPNSH/SPE (f). The interaction between AA and different double stranded DNAs leads to a significant decrease in CV signals (curve c–f) that is attributed to weak interaction between AA and different dsDNAs. But a significant CV signal is observed in the presence of G_4DNA (curve b) due to the intense interaction of AA/G_4DNA. This phenomenon can be explained in this way: guanine base of Gquadruplex can interact with *N*-propylpipyrazine-*N*-(2-mercaptopropane-1-one), which exists inside the channels of the mesoporous silica. Thus, a stable and non-physically adsorption takes place inside the channels. After adding AA, the interaction of G_4DNA with AA takes place in a nano-reactor that enhances the oxidation signal of AA significantly. In case of dsDNAs, the interaction between guanine bases with *N*-propylpipyrazine-*N*-(2-mercaptopropane-1-one) cannot happen well, because the cytosine bases in complementary strands form three stable hydrogen bonds with guanine bases. So, dsDNAs cannot stand in channel well. On the other hand, AA does not have a good interaction with dsDNAs which induces a decrease in AA oxidation current. These results further confirm that this biosensor selectively responds to the G_4DNA.

To make sure about this discussion, this study has done in the presence of different DNA molecules, too (Table 2). Fig. 5B shows CV signals of AA after immobilization of these DNA molecules. As can be seen, the interaction between AA and different single stranded and double stranded DNAs leads to a significant decrease in CV signals (curve c–h), too.

3.5. CD investigation of G_4DNA formation in solution

Circular dichroism (CD) spectra provide reliable information for identifying Gquadruplex structure, that is different from those of ssDNA, dsDNA or the other structures [28]. To make sure about forming of Gquadruplex structure, CD experiment was used before

Table 2
DNA molecules for selectivity study

DNA molecules	Structure
C53C (dsDNA)	TGG GGA TGG AGA ACT ACC CCT ACC TCT TGA y
G53g (dsDNA)	GTT ACT CTT GTA GAT ACT AC CAA TGA GAA CAT CTA TGA TG
HPV (dsDNA)	AGT TCT GCA TCC CCA TCA AGA CGT AGG GGT
C53C (ssDNA)	AGT TCT GCA TCC CCA
G53G (ssDNA)	TGG GGA TGC AGA ACT
PNA	AGT TCT CCA TCC CCA

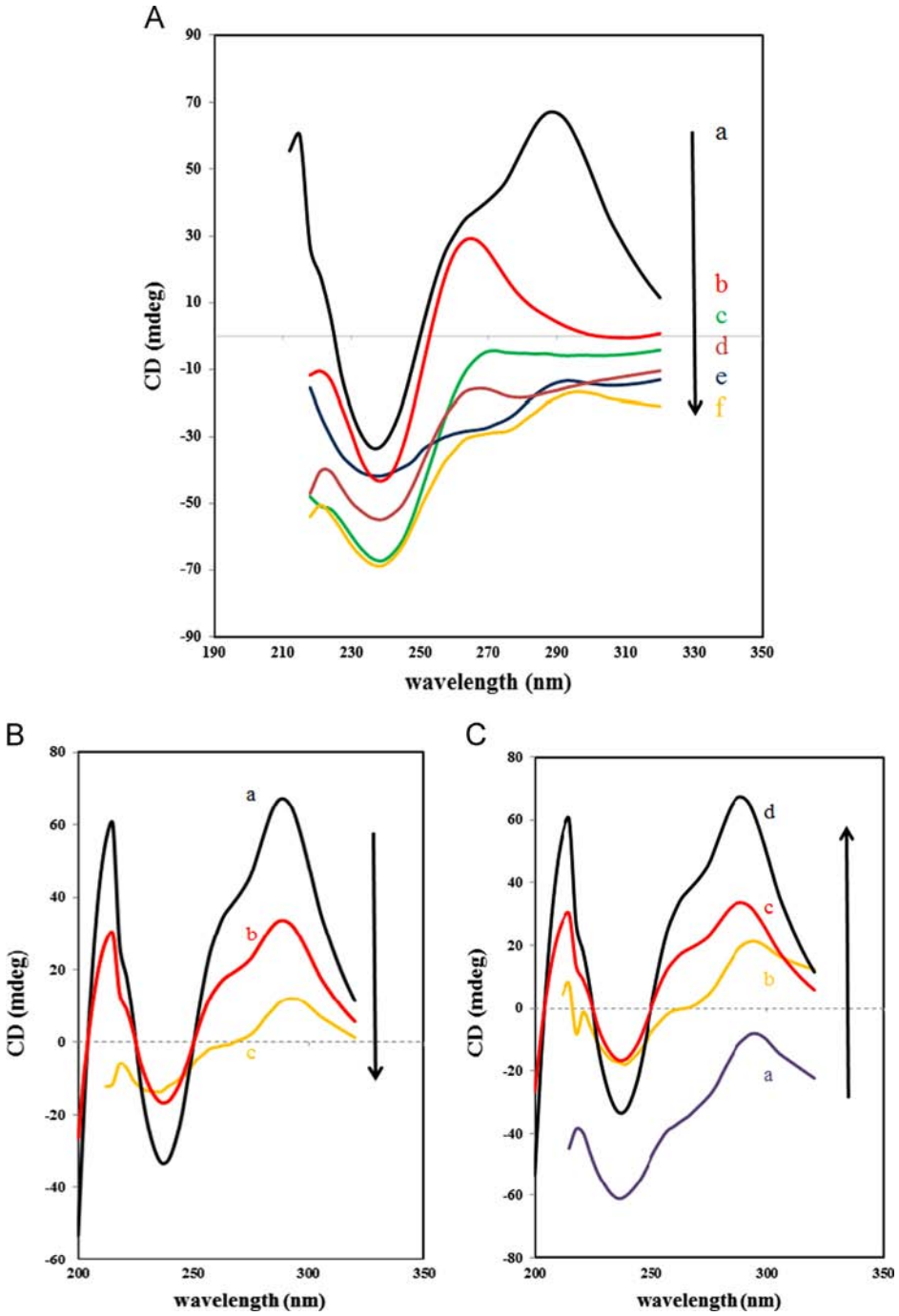

Fig. 6. CD spectrum of (A) 1.0 μmol L^{-1} G_4DNA (a), 1.0 μmol L^{-1} dsDNA (I) (b), 1.0 μmol L^{-1} dsDNA (II) (c), 1.0 μmol L^{-1} dsDNA (III) (d), 1.0 μmol L^{-1} dsDNA (IV) (e) and 1.0 μmol L^{-1} dsDNA (V) (f). (B) 1.0 μmol L^{-1} G_4DNA in the absence (a) and presence of different concentrations of AA: 1.0×10^{-7} mol L^{-1} (b) and 1.0×10^{-4} mol L^{-1} (c). (C) 1.0 μmol L^{-1} G_4DNA/SBA@NPPNSH in the absence (a) and presence of different concentrations of AA: 1.0×10^{-6} mol L^{-1} (b), 1.0×10^{-5} mol L^{-1} (c) and 1.0×10^{-4} mol L^{-1} (d).

any effort about G_4DNA immobilization on the surface of SBA@NPPNSH/SPE. CD spectra were recorded under this condition (50 mM Tris–HCl, 100 mmol L^{-1} KCl and 1.0 μmol L^{-1} G_4DNA at pH 7.40) and were compared with CD spectra of the other dsDNAs (50 mmol L^{-1} Tris–HCl, 1.0 μmol L^{-1} dsDNA at pH 7.40). Two basic CD spectra are usually observed for the Gquadruplex: the antiparallel type, which has a positive band around 295 nm and a negative band around 260 nm, and the parallel type, which exhibits a positive band around 265 nm and a negative band around 240 nm [29]. While linear human telomeric DNA shows a positive peak near 255 and a negative peak around 234 nm [30], the dsDNA structure shows a positive peak in 265 nm [31]. As can be seen in Fig. 6A (curve a), the human telomeric sequence shows folding topology with hybrid-type mixed parallel/antiparallel G-strands. The CD spectrum of the G_4DNA shows two CD bands. There is a positive band at 290 nm with a shoulder peak around 254 nm, and a negative band at 234 nm. This structure (hybrid-type folding) can be the most-favored for non-parallel-stranded intermolecular Gquadruplex with extended flanking sequences, according to the literature [32]. Fig. 6A (curve b–f), refers to the CD spectra of different dsDNAs. As it is clear, the CD spectra of

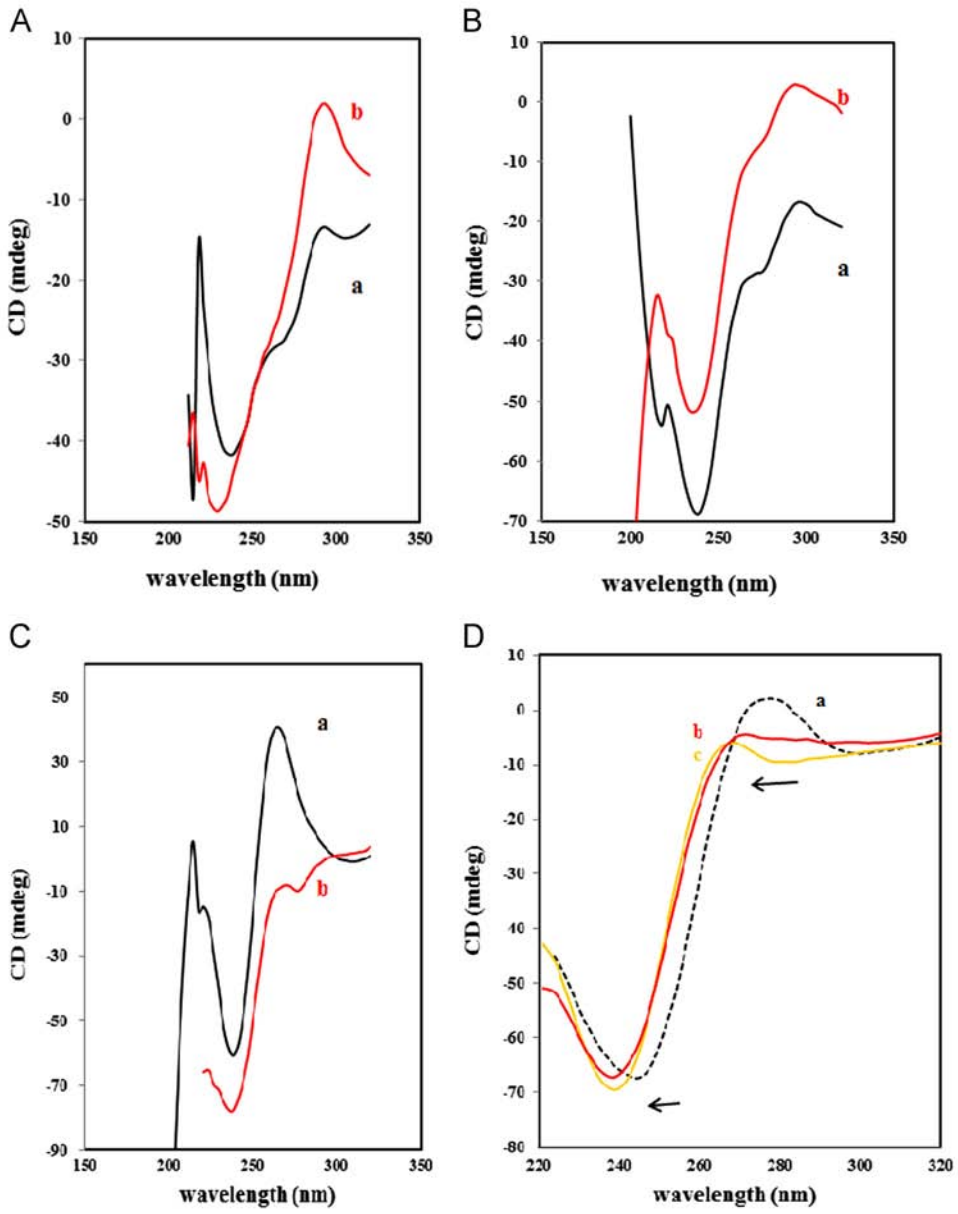

Fig. 7. CD spectrum of (A) 1.0 μmol L^{-1} dsDNA (V) in the absence (a) and presence of 1.0×10^{-5} mol L^{-1} of AA (b), (B) 1.0 μmol L^{-1} dsDNA (IV) in the absence (a) and presence of 1.0×10^{-5} mol L^{-1} of AA (b), (C) 1.0 μmol L^{-1} dsDNA (II) in the absence (a) and presence of 1.0×10^{-5} mol L^{-1} of AA (b), and (D) 1.0 μmol L^{-1} dsDNA (I) in the absence (a) and the presence of 1.0×10^{-6} mol L^{-1} of AA (b) and 1.0×10^{-5} mol L^{-1} of AA (c).

dsDNA (I), (II) and (III) show the positive characteristic peak in 265 nm, but the CD spectra of dsDNA (IV) and (V) show the G_4DNA-like structure.

3.6. *The effect of G_4DNA/AA interaction on the CD spectra*

Fig. 6B shows CD spectra of G_4DNA in the presence of different concentrations of AA (10^{-7}–10^{-4} mol L^{-1}). It is observed that the spectra of G_4DNA exhibit a dramatic increase in the negative band at 234 and a decrease in the positive band at 290 nm and the shoulder peak around 255 nm (curves b–c). It is concluded from the CD spectra that AA has an intense interaction with G_4DNA, but it cannot change the position of G_4DNA peak strongly. Therefore, the interaction mode between G_4DNA and AA has probably been intercalation, according to the literature [33–35]. To obtain more information, these measurements have been done in the presence of SBA@NPPNSH. The CD spectra of G_4DNA/SBA@NPPNSH were recorded before and after addition of different concentrations of AA. Fig. 6C shows the CD spectra of G_4DNA/SBA@NPPNSH in the absence (curve a) and in the presence of different concentrations of AA (curve b–d). As it illustrates clearly, CD spectra increase with increasing AA concentration, that is different from the results obtained in the absence of SBA@NPPNSH. As it was explained, G_4DNA can place in the nano-size channels of SBA@NPPNSH structure, so the CD spectra of G_4DNA decrease in the presence of SBA@NPPNSH after addition of ligand. AA can interact with

G_4DNA structure and increase its stability, so the CD spectra increase, which confirms the stability effect of AA on Gquadruplex DNA structure.

In order to make more information, the CD spectra of different dsDNAs were recorded in the absence and presence of AA. Fig. 7(A) shows the CD spectra of dsDNA (V) in the presence of 1.0×10^{-5} mol L^{-1} AA in 50 mmol L^{-1} Tris–HCl buffer. Without AA, the CD spectra of the dsDNA (V) exhibit a positive peak at 295 nm and a negative peak around 240 nm at room temperature. Upon the addition of AA to the solution, a dramatic change in the CD spectrum is observed. The maximum at 295 nm is gradually increased, while the negative peak decreased dramatically along with the increase of the AA concentration. It shows that the Gquadruplex structure becomes more stabilized in the presence of AA. The CD spectra of dsDNA (IV) exhibit similar results with dsDNA (V) (Fig. 7B). The CD spectra of dsDNA (III), in the presence of 1.0×10^{-5} mol L^{-1} AA in 50 mmol L^{-1} Tris–HCl buffer, is shown in Fig. 7C. A positive peak is observed near 265 nm for dsDNA (III) in the absence of AA. Upon addition of AA to the solution, the maximum at 265 nm is gradually decreased, while a positive peak at about 295 is observed which is related to human telomeric DNA structure. As can be seen, the CD spectra of dsDNA (I) (complementary strand) in the absence of AA shows a positive peak about 275 nm and a negative band around 250 nm. In the presence of AA, the positive peak shifts to 265 nm and the negative peak shifts to 240 nm, that is related to parallel type of G_4DNA structure.

These results clearly show that AA can stabilize G_4DNA structure. It can induce the short complementary strand to make the human telomeric Gquadruplex structure and also induce the completely complementary strands to make the parallel G_4DNA structure and reduce the stability of dsDNAs.

4. Conclusion

The SBA@NPPNSH modified graphite SPE have been employed as a good nanostructure platform for the construction of a G_4DNA biosensor by good biocompatibility, suitable electroactivity and high specific surface area. Ascorbic acid has been introduced as a new ligand to stabilize the Gquadruplex structure of human telomeric DNA sequences that is important in cancer therapy and genomic study. The mechanism of G_4DNA/AA interaction has been studied using cyclic voltammetry and CD spectroscopy methods. Data from CD spectroscopy have indicated that AA can reduce the stability of DNA duplexes which leads to G_4DNA formation. So, AA can have antitumor activity by inhibiting the telomerase enzyme activity. The advantages of the proposed biosensor are rapid detection and the ability to distinguish G_4DNA from dsDNA structure at physiological pH. Reports from our laboratory are in progress toward the usage of this ligand for antitumor activity in extracted DNA genome as real sample.

Appendix A. Supplementary material

Supplementary data associated with this article can be found in the online version at http://dx.doi.org/10.1016/j.talanta.2013.09.052.

References

[1] E.H. Blackburn, Cell 106 (2001) 661–673.
[2] C.W. Greider, Proc. Natl. Acad. Sci. USA 95 (1998) 90–92.
[3] A.T. Phan, FEBS J. 277 (2010) 1107–1117.
[4] A.M. Zahler, J.R. Williamson, T.R. Cech, D.M. Prescott, Nature 350 (1991) 718–720.
[5] S. Neidle, G. Parkinson, Nat. Rev. Drug Discovery 1 (2002) 383–393.
[6] G. Zheng, W.L. Daniel, C.A. Mirkin, J. Am. Chem. Soc. 130 (2008) 9644–9645.
[7] C.C. Hardin, E. Henderson, T. Watson, J.K. Prosser, Biochemistry 30 (1991) 4460–4472.
[8] C.C. Hardin, T. Watson, M. Corregan, C. Bailey, Biochemistry 31 (1992) 833–841.
[9] L.H. Hurley, Nat. Rev. Cancer 2 (2002) 188–200.
[10] R.H. Shafer, I. Smirnov, Biopolymers 56 (2000) 209–227.
[11] S. Neidle, M.A. Read, Biopolymers 56 (2000) 195–208.
[12] H. Sun, R.J. Bennett, N. Maizels, Nucleic Acids Res. 27 (1999) 1978–1984.
[13] L. Oganesian, T.M. Bryan, BioEssays 29 (2007) 155–165.
[14] Y. Wu, R.M. Brosh, FEBS J. 277 (2010) 3470–3488.
[15] L.H. Hurley, R.T. Wheelhouse, D. Sun, S.M. Kerwin, M. Salazar, O.Y. Fedoroff, F.X. Han, H. Han, E. Izbicka, D.D. Von Hoff, Pharmacol. Ther. 85 (2000) 141–158.
[16] S. Cogoi, L.E. Xodo, Nucleic Acids Res. 34 (2006) 2536–2549.
[17] M. Lachapelle, G. Drouin, Genetica 139 (2011) 199–207.
[18] R.O. Kadara, N. Jenkinson, C.E. Banks, Sens. Actuat. B—Chem. 138 (2009) 556–562.
[19] M. Tudorache, C. Bala, Anal. Bioanal. Chem. 388 (2007) 565–578.
[20] Y. Zhao, Z.-Y. Kan, Z.-X. Zeng, Y.-H. Hao, H. Chen, Z. Tan, J. Am. Chem. Soc. 126 (2004) 13255–13264.
[21] J. Ruiz-Chica, M.A. Medina, F. Sánchez-Jiménez, F.J. Ramırez, BBA—Gene Struct. Expression 1628 (2003) 11–21.
[22] S. Laschi, I. Palchetti, G. Marrazza, M. Mascini, J. Electroanal. Chem. 593 (2006) 211–218.
[23] C. Yu, J. Fan, B. Tian, D. Zhao, G.D. Stucky, Adv. Mater. 14 (2002) 1742–1745.
[24] R.K. Dey, T. Patnaik, V.K. Singh, S.K. Swain, C. Airoldi, Appl. Surf. Sci. 255 (2009) 8176–8182.
[25] D. Zhao, Q. Huo, J. Feng, B.F. Chmelka, G.D. Stucky, Nonionic Triblock, J. Am. Chem. Soc. 120 (1998) 6024–6036.
[26] M.S. Ibrahim, Anal. Chim. Acta 443 (2001) 63–72.
[27] L. Wang, L. Lin, B. Ye, J. Pharm. Biomed. Anal. 42 (2006) 625–629.
[28] S. Nagatoishi, Y. Tanaka, K. Tsumoto, Biochem. Biophys. Res. Commun. 352 (2007) 812–817.
[29] J.R. Williamson, Annu. Rev. Biophys. Biomol. Struct. 23 (1994) 703–730.
[30] R. Jin, B.L. Gaffney, C. Wang, R.A. Jones, K.J. Breslauer, Thermodynamics and structure of a DNA tetraplex: a spectroscopic and calorimetric study of the tetramolecular complexes of d(TG3T) and d(TG3T2G3T), in: Proceedings of the National Academy of Sciences of the USA 89, 1992, pp. 8832–8836.
[31] W. Li, D. Miyoshi, S.-I. Nakano, N. Sugimoto, Biochemistry 42 (2003) 11736–11744.
[32] A. Ambrus, D. Chen, J. Dai, T. Bialis, R.A. Jones, D. Yang, Nucleic Acids Res. 34 (2006) 2723–2735.
[33] U. Sehlstedt, S.K. Kim, P. Carter, J. Goodisman, J.F. Vollano, B. Norden, J.C. Dabrowiak, Biochemistry 33 (1994) 417–426.
[34] I. Lubitz, N. Borovok, A. Kotlyar, Biochemistry 46 (2007) 12925–12929.
[35] B. Ward, A. Skorobogaty, J.C. Dabrowiak, Biochemistry 25 (1986) 7827–7833.